Alexandria Engineering Journal (2018) 57, 2975–2989

HOSTED BY

ELSEVIER

Alexandria University

Alexandria Engineering Journal

www.elsevier.com/locate/aej
www.sciencedirect.com

ORIGINAL ARTICLE

Numerical and experimental study of the influence of nozzle flow parameters on yarn production by jet-ring spinning

Hassan A.H. Ahmed [a,*], **Rola S. Afify** [b], **Ahmed H. Hassanin** [a], **Ibrahim A. El-Hawary** [a], **Raafat I. Mashaly** [a]

[a] *Textile Department, Faculty of Engineering, Alexandria University, Alexandria, Egypt*
[b] *Mechanical Engineering Department, Faculty of Engineering, Arab Academy for Science, Technology and Maritime Transport (AAST), Abu kir, Alexandria, Egypt*

Received 7 March 2017; revised 24 January 2018; accepted 26 June 2018
Available online 22 November 2018

KEYWORDS

Jet-ring spinning;
Yarn hairiness;
CFD;
Simulation;
Air jet nozzle

Abstract Yarn hairiness is defined as the protruding fibers and loops standing out of the core of the yarns. Effect of yarn hairiness on different post processes, and its influence on the characteristics of the product obtained, has led to attempts at reducing hairiness. In recent years, new technologies such as compact spinning, solo spinning and jet-ring spinning have been developed to reduce the hairiness of ring spun yarn. In this paper, a Computational Fluid Dynamics (CFD) model is presented to study the effects of some air jet nozzle structural parameters as injector angle, nozzle length, and air pressure level on the swirling flow generated inside the nozzle. Followed by design and construction of a mechanism for producing jet ring and modified jet ring yarns. Finally, an experimental study on the effects of some nozzles and air flow parameters on jet ring and modified jet ring yarn properties is presented intending to illustrate the role of inserting the air jet nozzle for improving these systems.

1. Introduction

Yarn hairiness is a significant parameter of spun yarns quality [1]. It influences the quality of yarn, as well as the sewing and weaving behavior of yarns and, additionally, the resultant fabrics quality [2]. Different improvements, with respect to yarn hairiness, have been developed in the most recent decade [3,4]. These spread aspects like testing of hairiness, simulation, modeling, spinning developments and next spinning handling to reduce hairiness [5–9].Overall yarn properties can be enhanced by introducing simple devices, like air jet nozzle [10–13], on traditional ring spinning machine to improve a developed system as jet-ring spinning [14,15].

The Jet-ring spinning or Nozzle-Ring spinning technique [16,17] is a new technique which combines both features of conventional ring and air-jet spinning technology. A single nozzle was placed below the yarn formation zone andacted in a way similar to the first nozzle used in air-jet spinning.

* Corresponding author.
E-mail address: hassanthefuture1@yahoo.com (H.A.H. Ahmed).
Peer review under responsibility of Faculty of Engineering, Alexandria University.

https://doi.org/10.1016/j.aej.2018.06.002
1110-0168 © 2018 Faculty of Engineering, Alexandria University. Production and hosting by Elsevier B.V.

The swirling air flow inside the nozzle was capable of wrapping the protruding hairs around the yarn body, thereby reducing yarn hairiness.

Subramaniana et al. [18] used 100% cotton for producing yarn count about 20 Tex. They fabricated single, double and triple air jet nozzles using Teflon, aluminum and brass materials. The geometrical parameters of nozzle were as following: nozzles length were (25, 75, and 115 mm) respectively for single, double and triple nozzles, jet injector angle was (45°), and main hole diameter was (3.5 mm). Jet ring yarns had higher tenacity and lower yarn hairiness (H and S3 values) than normal ring spun yarns for all count of yarns.

Nowadays, Computational Fluid Dynamics (CFD) is widely used in textile technology to analyze processes that involve fast and complicated movements of fibers and yarns or fabrics, for examples, air jet spinning, air jet texturing, air jet weaving, air vortex spinning and a range of finishing processes. Before the possibility of utilizing CFD, most of these technologies were developed well. Now, it is possible to improve those technologies by taking a closer look, which was unimaginable before 1998 [19].

Hasani, and Hasani [20] simulated the air flow pattern inside the air jet nozzle. They applied Fluent 6.10 (finite volume method and fluid flow analysis package program) for flow simulation. They considered the following assumptions for the simulation; the flow in the jets was turbulent, the yarn was not modeled because its presence has no effect on the flow patterns, the high velocity of the air flow is a heat source that will increase the temperature in the jet nozzles, the jet nozzle is very small and the action occurs very quickly and the process is assumed to be adiabatic, i.e. with no heat transfer through walls. They chose standard k-ε as a turbulence model. They found that using of an air jet nozzle that had higher orifice inclination gave a higher tangential velocity, which can result in an unsteady motion, yarn ballooning and air jet nozzle efficiency reduction. The air pressure effect was also examined; they found that an increase in air pressure level can lead to a higher tangential, axial, and radial velocity. This increase in velocity will depend on the air jet nozzle geometry.

Rengasamy et al. [21] notified, on hairiness reduction using air jet nozzle in traditional ring spinning based on CFD, that air drag forces and angle of impact of air on hair played a significant role in jet ring spinning system. Airflow behavior inside the nozzle was modeled by a fluid flow analysis program, Fluent 6.1 was used to solve the 3D airflow field inside the nozzles. The profile of airflow was simulated using a CFD model and drag forces acting on hair were computed. They found that the hairiness reduction was affected by the air drag forces level acting on the hairs.

Patnaik et al. [22] stated that airflow simulation inside nozzles showed some concepts into hairiness reduction mechanism. That was through the examination of hairiness control using nozzles at ring frame. A CFD model was developed in order to solve the 3D airflow pattern inside the nozzles and simulate the airflow behavior inside the nozzles using FLUENT 6.1 program. They investigated the effect of nozzle parameters as orifice angle, yarn main hole diameter, and yarn count on the reduction of hairiness.

Yilmaz and Usal [23] simulated the pressurized air inside a nozzle by ANSYS 12.1 program and Fluid Flow (CFX) analysis method. Two types of nozzles were studied to resolve the airflow structure and its effect on yarn properties. For the first nozzle (normal type), orifice was put close to nozzle opening. For the second type (center positioned nozzle), orifice was placed in middle of the nozzle. An air pressure of 0.5 bar was used. "Shear Stress Transport (SST)" turbulent model was selected; this is a one of the Reynolds stress models, as a solution algorithm. They stated that air velocity values of normal positioned nozzle were higher than that of center positioned. While normal positioned nozzle had lower velocity values at the nozzle exit. Velocity values of airflow at the orifices were higher than that of the other components of the nozzle. In addition to that its velocity decreased along the nozzle. The airflow exit from the nozzle outlet with lower distance at center positioned nozzle, hence airflow velocity was higher.

Guo et al. [24] introduced the computational domain that was the main hole of the nozzle from opening to exit, including orifices and slotting tubes. They stated that standard k-ε two- equation turbulence model has been widely applied to engineering practice, but it was criticized as being only qualitatively correct in the simulation of confined swirling flows. This was because of the neglect of anisotropic viscosity and additional turbulence generation arising from the effects of streamline curvature in the standard k-ε model. They stated that the realizable k-ε turbulence model is an eddy viscosity model, which consists of a new model dissipation rate equation and a new realizable eddy viscosity formulation. They used realizable k-ε model to simulate flow structure in the nozzle with slotting-tube, because it has shown some improvements on standard k-ε model where the flow features included strong streamline curvature, vortices and recirculation. They demonstrated the functions of the slotting-tube. Also, they discussed the effect of nozzle pressures on the flow characteristics and yarn properties.

The first purpose of this paper is to study, analyze, predict, and control the effect of swirling air flow behavior on the fibers movement and yarns properties. The second objective is using the air-jet nozzle in ring spinning system to produce a jet ring yarn with superior quality especially yarn strength and yarn hairiness, and hence improve the post process efficiency. The plan of work is to achieve these purposed objectives. First, set-up a CFD model to simulate the air flow behavior inside air jet nozzles, and study the effects of some jet nozzle structural parameters on the swirling flow generated inside the nozzle. Second, design and construct a mechanism for producing jet ring and modified jet ring yarns. Third, experimental study of the effect of some nozzles and yarn parameters on jet ring and modified jet ring yarn properties aiming to illustrate the role of inserting the air jet nozzle in different positions for improving these systems and their products quality.

2. Simulation for air flow inside jet nozzle using CFD

To understand swirling air flow behavior inside air jet nozzles, air flow structure inside the nozzle was analyzed using ANSYS 14, a package program with fluid flow (FLUENT) analysis method. The experimental design for the effect of nozzle length, injector's vertical angles of the nozzle Θ and air pressure were carried out.

The nozzles are designed in two main categories, short nozzles with length 12.0 mm and long nozzles with length 24.0 mm each nozzle has four tangential air inlets (injectors) placed in the center of the nozzle with constant orifice diameter

0.5 mm but with different angles with respect to the nozzle axis. The vertical angles of the injector's Θ are 15°, 25°, 35°, 45°, 55°, each nozzle has constant cylindrical cross section with a diameter 2.0 mm, and it is assumed that the cross sectional area of the yarn is about 1/100th of the inner hole of the nozzle and the yarn occupied a small area in the nozzle. Hence, the flow inside the nozzle affected the yarn, but not vice versa. Therefore, the yarn is not modeled in the numerical analysis. Long and short nozzles profiles are shown in Figs. 1 and 2. The nozzles are meshed by tetrahedron meshing method, patch independent with a finite volumes varying from 99,000 and 130,000 elements, shown in Figs. 3 and 4.

2.1. Boundary conditions

The boundaries condition of nozzle, shown in Fig. 5, consists of the following:

- Injectors: are assumed to be (pressure inlet) with different values 0.5, 1, 1.5, 2, 2.5, 3 bar.
- Main inlet: from which the yarn entered the domain, so, it is considered as (pressure inlet) with atmospheric pressure condition.
- Outlet: the nozzle outlet is considered to be (pressure outlet) with atmospheric condition.
- All the rest of the boundaries are automatically considered as walls with non-slip boundary conditions.

The solver type is chosen to be pressure-based. Shear Stress Transport (SST) (K-ω) turbulence model is used as a solution algorithm. It is one of the Reynolds stress models. It accounts for the transport of the turbulent shear stress and gives highly accurate predictions of the onset and the amount of the flow separation under adverse pressure gradients. The shear-stress transport (SST) (k-ω) model, so named because the definition of the turbulent viscosity is modified to account for the transport of the principal turbulent shear stress. It is this feature that gives the SST k-ω model an advantage in terms of performance over both the standard k- ω model and the standard k-ε model. Other modifications include the addition of a cross-diffusion term in the w equation and a blending function to ensure that the model equations behave appropriately in the both the near-wall and far-field zones [25], the transport equations for SST k-ω model are

Turbulence kinetic energy equation

$$\frac{\partial k}{\partial t} + \bar{u}_j \frac{\partial k}{\partial x_j} = P_k - \beta^* k\omega + \frac{\partial}{\partial x_j}\left[(\upsilon + \sigma_k \upsilon_T)\frac{\partial k}{\partial x_j}\right]$$

Specific dissipation rate equation

$$\frac{\partial \omega}{\partial t} + \bar{u}_j \frac{\partial \omega}{\partial x_j} = \alpha S^2 - \beta\omega^2 + \frac{\partial}{\partial x_j}\left[(\upsilon + \sigma_w \upsilon_T)\frac{\partial \omega}{\partial x_j}\right] + 2(1 - F_1)\sigma_{w2}\frac{1}{\omega}\frac{\partial k}{\partial x_i}\frac{\partial \omega}{\partial x_i}$$

Kinematic eddy viscosity equation $\upsilon_T = \frac{\alpha_1 k}{\max(\alpha_1 \omega, SF_2)}$

The closure coefficients and auxiliary relations are:

$$F_2 = \tanh\left\{\left[\max\left(\frac{2\sqrt{k}}{\beta^* \omega y}, \frac{500\upsilon}{y^2\omega}\right)\right]^2\right\},$$

$$P_k = \min\left(\tau_{ij}\frac{\partial \bar{u}_i}{\partial x_j}, 10\beta^* k\omega\right),$$

$$F_1 = \tanh\left\{\left\{\min\left[\max\left(\frac{\sqrt{k}}{\beta^* \omega y}, \frac{500\upsilon}{y^2\omega}\right), \frac{4\sigma_{w2}k}{CD_{kw}y^2}\right]\right\}^4\right\},$$

$$CD_{kw} = \max\left(2\rho\sigma_{w2}\frac{1}{\omega}\frac{\partial k}{\partial x_i}\frac{\partial \omega}{\partial x_i}, 10^{-10}\right),$$

$\phi = \phi_1 F_1 + \phi_2(1 - F_1)$ (as $\phi = \alpha, \beta, \sigma_k, \sigma_w$, $\phi_1 = \alpha_1, \beta_1, \sigma_{k1}, \sigma_{w1}$, and $\phi_2 = \alpha_2, \beta_2, \sigma_{k2}, \sigma_{w2}$)

$$\alpha_1 = \frac{5}{9},\ \alpha_2 = 0.44,\ \beta_1 = \frac{3}{40},\ \beta_2 = 0.0828,\ \beta_o^* = 0.09,$$

$$\sigma_{k1} = 0.85,\ \sigma_{k2} = 1,\ \sigma_{w1} = 0.5,\ \sigma_{w2} = 0.856$$

The used fluid is air and is specified as ideal gas (compressible fluid). The process was considered as adiabatic (i.e. with no heat transfer through wall). Solution method scheme is set to be (SIMPLEC). A pressure based solver is used. The gradients of solution variables at cell centers are determined using "least squares cell based" approach. Solution initialization method is chosen to be Hybrid Initialization. Sensitivity of the solution was set at 10^{-5}.

3. Results and discussions of analysis of ANSYS fluid flow (FLUENT)

Different types of airflow results arise with different nozzle angles, lengths, and air pressures.

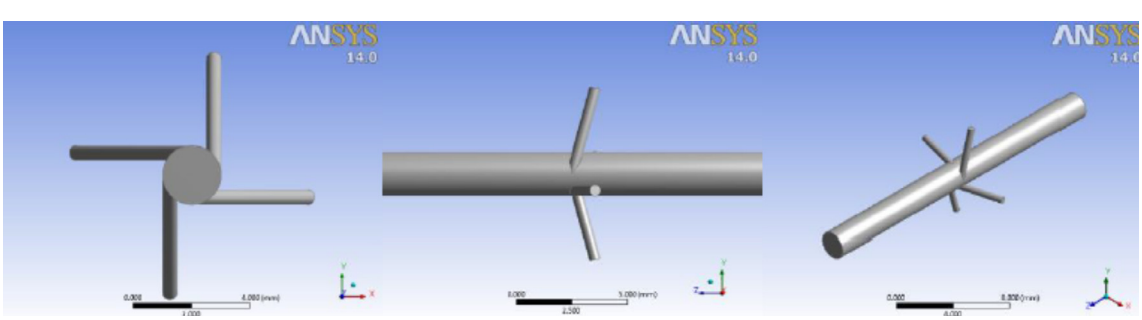

Fig. 1 Long nozzle profiles with injector vertical angle 15°.

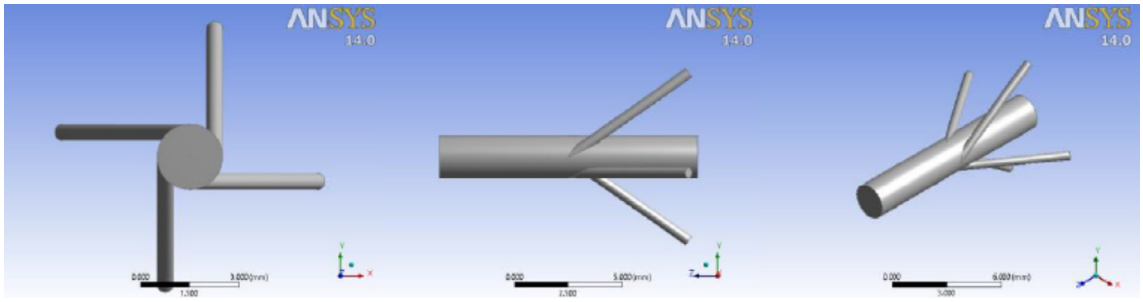

Fig. 2 Short nozzle profiles with injector vertical angle 55°.

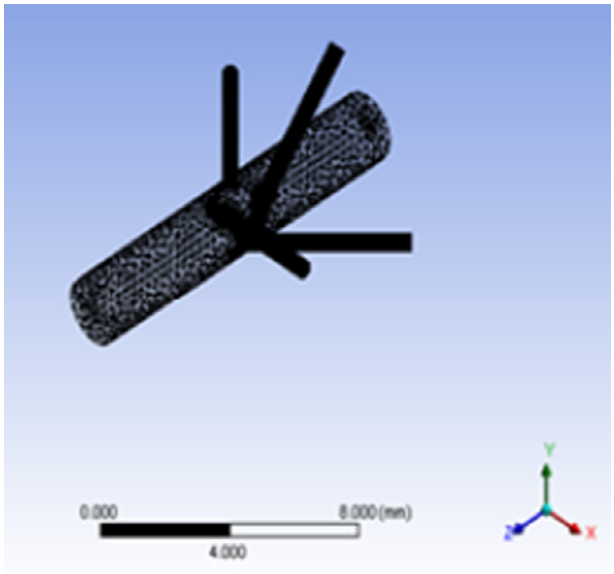

Fig. 3 Grid structures of short nozzle.

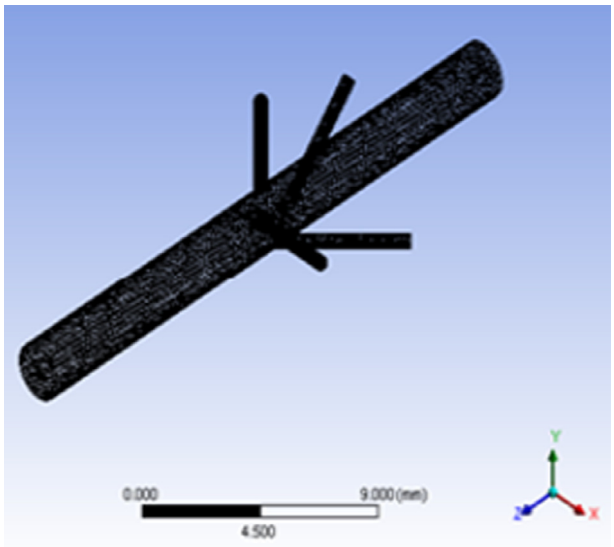

Fig. 4 Grid structures of long nozzle.

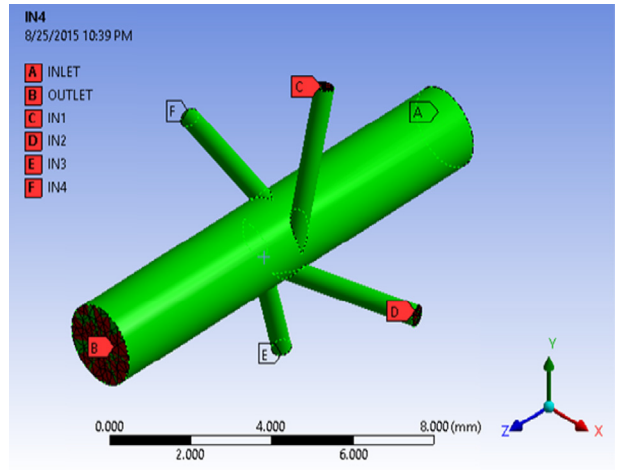

Fig. 5 Boundaries conditions of nozzle.

3.1. Flow streamlines

The figures from 6 to 9 generally indicate the air flow behavior inside the nozzle through representing the air velocities with streamlines colored with its magnitude.

Fig. 6 shows the Airflow behavior inside the long nozzle with injector vertical angle 15° with different air pressures from 0.5 to 3 bar. The air flow pattern is divided into three main parts; the first is the air flow, which sent from injectors into the main nozzle hole. This creates the pressurized air swirls along the nozzle. The rotating air flow moves in two directions towards the nozzle inlet and outlet around nozzle axis. As the angle increases, the amount of the air flow moving into nozzle inlet is lower. The second part is the air flow at nozzle inlet. Some air is sucked from the nozzle outlet. Then it starts to act into the nozzle leaving the nozzle domain from the nozzle outlet at air pressure 0.5 bar. While by increasing the air pressure values, the sucked air enters the nozzle domain till a certain distance, and then flows back to the nozzle inlet. This distance decreases by increasing the air pressure as shown in Fig. 6 from 1 bar to 3 bar. The third part, the air flow behavior at the nozzle outlet opening in which the air flow leaves the nozzle domain from nozzle outlet, no reversing flow is observed.

Fig. 7 shows the Airflow behavior inside the long nozzle with injector vertical angle 35° with different air pressures from 1 to 3 bar. At the first part, the air flow is sent from injectors into the main nozzle hole creating an air vortex at approx-

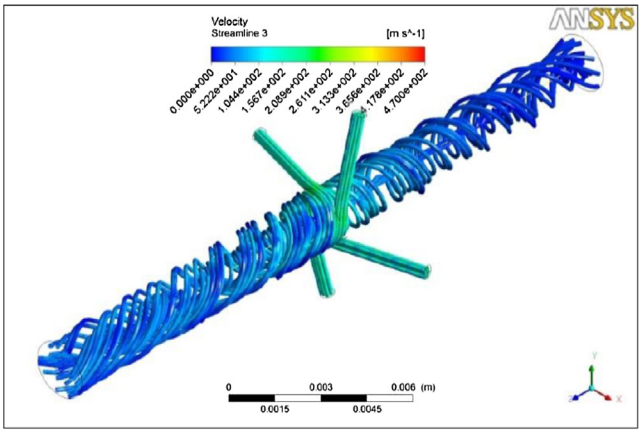

a- 0.5 bar

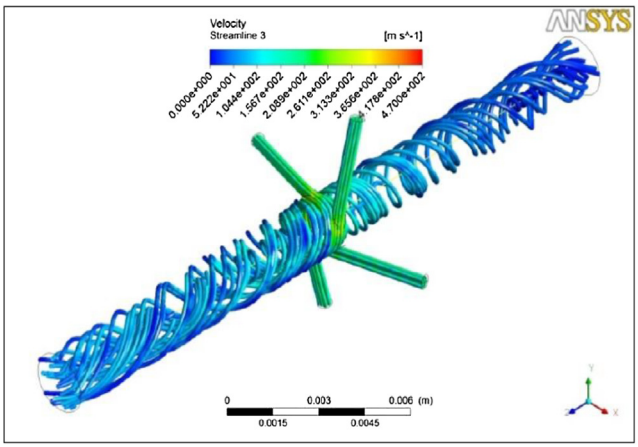

b- 1 bar

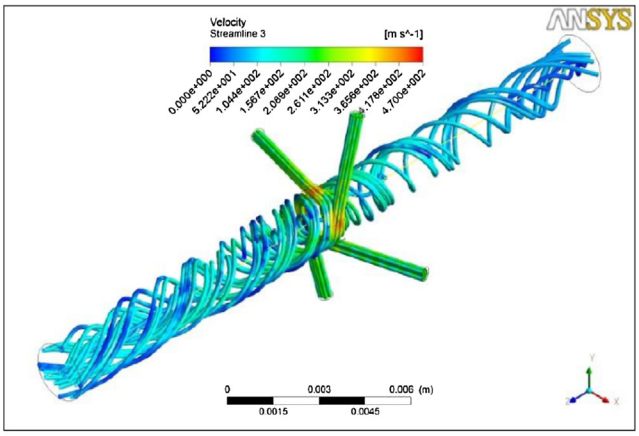

c- 2.5 bar

Fig. 6 Airflow behaviors inside the nozzle for different air pressure (long nozzle – injector vertical angle 15°).

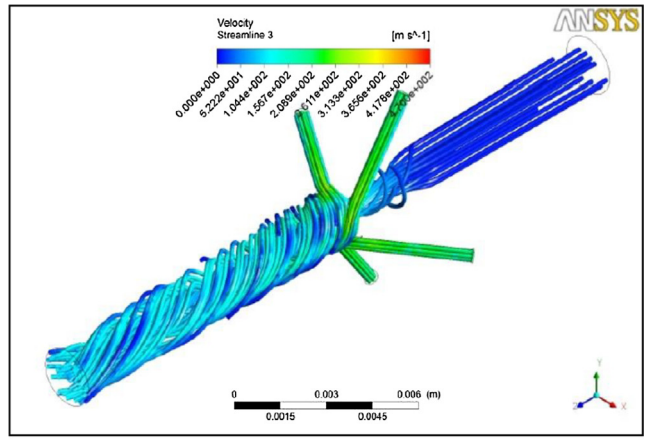

a- 1 bar

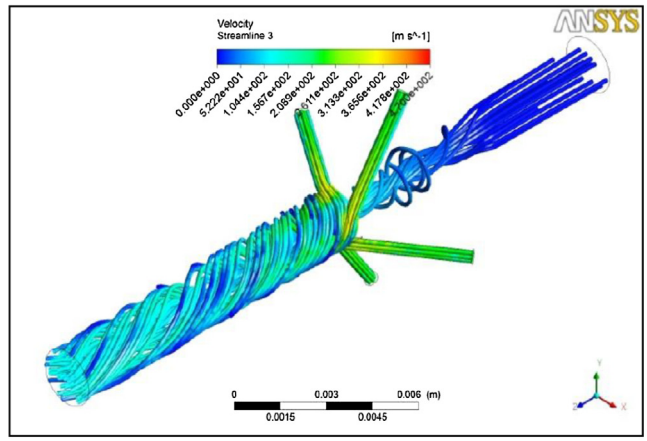

b- 2 bar

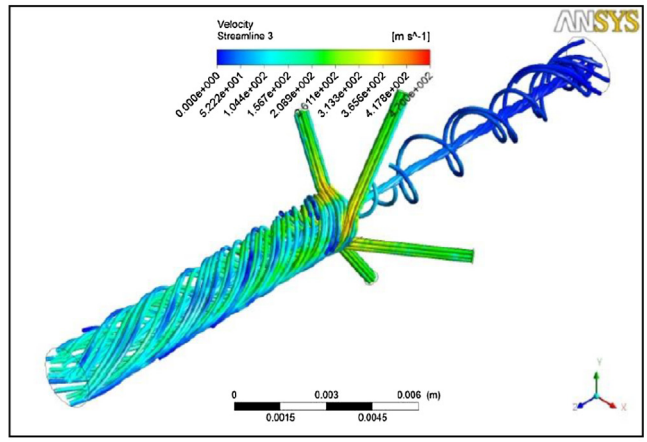

c- 3 bar

Fig. 7 Airflow behaviors inside the nozzle for different air pressure (long nozzle – injector vertical angle 35°).

imately the middle of the nozzle acting with a swirling motion around nozzle axis reaching the nozzle outlet. In addition, a quite reversed air flow swirling motion towards the nozzle inlet was observed, then it returns back to nozzle outlet. This reversed motion increases by increasing the air pressure values, but at air pressure value 3 bar it leaves the nozzle domain from nozzle inlet. in the second part of the air flow, at nozzle inlet some air is sucked from the nozzle outside, and then it starts to act into the nozzle with straight streamlines parallel to the nozzle axis till a certain distance then it moves in a swirling motion near the nozzle center, leaving the nozzle domain from the nozzle outlet, as shown in cases of air pressure from 1 to

2 bar. While increasing the air pressure values, the sucked air enters the nozzle domain is lower with swirling motion from nozzle inlet to nozzle outlet as shown in cases air pressure from 2.5 to 3 bar. At the third part, the flow leaves the nozzle domain from nozzle outlet, and no reverse flow was observed (same as in previous nozzles).

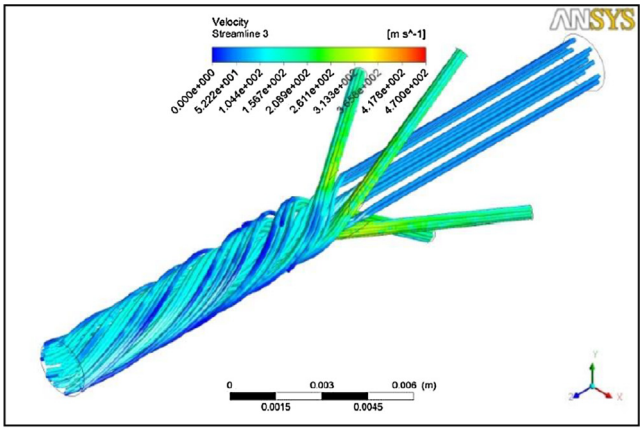

a- 1 bar

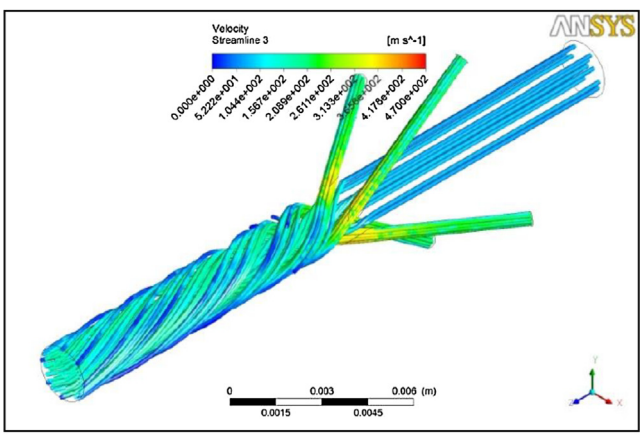

b- 2 bar

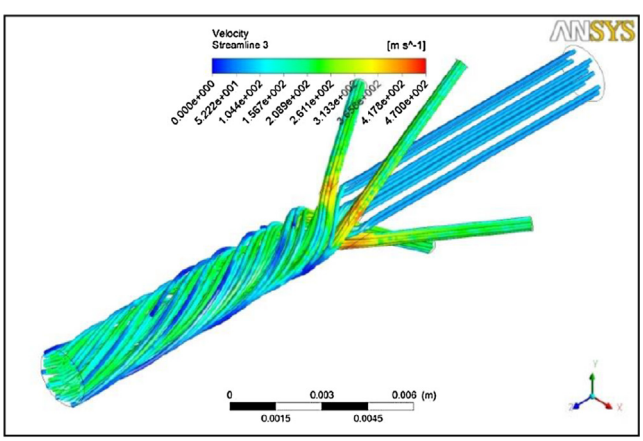

c- 3 bar

Fig. 8 Airflow behaviors inside the nozzle for different air pressure (long nozzle – injector vertical angle 55°).

Fig. 8 shows the Airflow behavior inside the long nozzle with injector vertical angle 55° with different air pressures from 1 to 3 bar. At the first part, the air flow is similar to air flow behavior of the long nozzle with angle 45° but it moves with lower intensive swirling motion. In the second part, the air flow at nozzle inlet is similar to the air flow behavior of the long nozzle with angle 45° but the parallel straight stream lines are wider to each others. At the third part, the flow leaves the nozzle domain from nozzle outlet, no reverse flow was observed (same as in previous nozzles).

Fig. 9 shows the Airflow behavior inside the short nozzle with injector vertical angle 15° with different air pressures from 1 to 3 bar. At the first part, the air flow is as same as the air flow behavior of the long nozzle with angle 15°. In the second part, the air flow at nozzle inlet is similar to the air flow behavior of the long nozzle with angle 15° but the swirling motion becomes wider and moves near to the inner wall of the nozzle until reaching nozzle outlet. In addition, some reversed air flows are observed leaving the domain from nozzle inlet. These air flows' amounts increase by increasing air pressure values, as shown in the figure. At the third part, the flow leaves the nozzle domain from nozzle outlet, but some reversed flows were observed. The distances of the reversed flows decrease with increasing the pressure values. As the angle increases, the distances of the reversed flows are lower with the same pressure values. For nozzle with injector vertical angle 45° and 55°, the air flow behavior is as same as in long nozzle with angle 55° in all the parts.

3.2. Contour of air flow axial velocity

Figs. 10–12 show the contours for long and short nozzles with different pressure values from 0.5 to 3 bar at ZY plane located along X = 0. The figures indicate that the general phenomenon for the air flow for all nozzles is that air enters the domain from the injectors in the middle of the nozzle reaching its maximum axial velocity at the core. Then the flow acts inside the nozzles with higher axial velocity at the peripheral than the flow at the core. By increasing the air pressure, the axial velocity magnitude increases. The axial velocity's negative values confirm the presence of reversed flows.

Fig. 10 shows the air flow axial velocity contours for long nozzle with injector vertical angle 15° with different air pressure values from (a) 0.5 bar to (f) 3 bar. In the first part, from nozzle inlet to middle, the flow has two directions; one is a reversed flow at the peripheral exit the domain from nozzle inlet, and the other is the sucked flow from outside into the core of the nozzle under the effect of the swirling action from injectors. By increasing the pressure values, the reversed mass flow at the peripheral increases preventing the sucked mass flow from entering the domain that leads to decrease the entered mass flow. At the second part, from middle of nozzle to outlet, a contour of a negative axial velocity value appears in the zone after the injectors towards the nozzle outlet. This contour reveals the presence of an Internal Recirculation Zone (IRZ) [24] generated as a result of the adverse pressure gradient at the core created by the swirl. By increasing the pressure values, the area of the IRZ decreases but its negative velocity value increases.

For injector vertical angles higher than 25°, all the contours at second part have positive values, no reversed flow occurred,

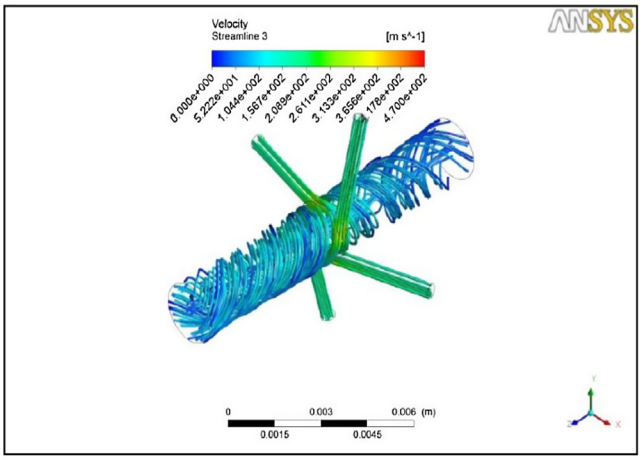

a- 1 bar

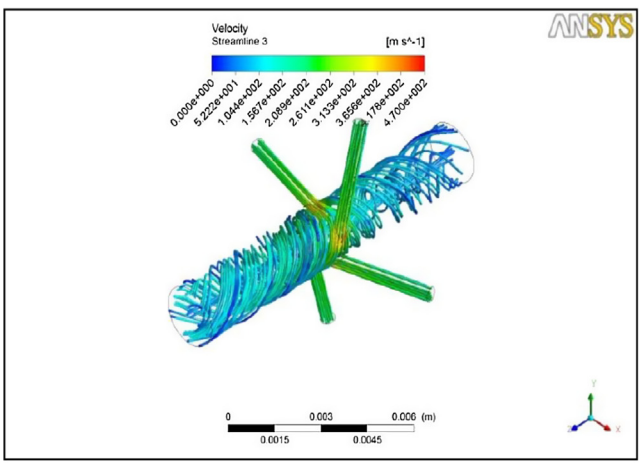

b- 2 bar

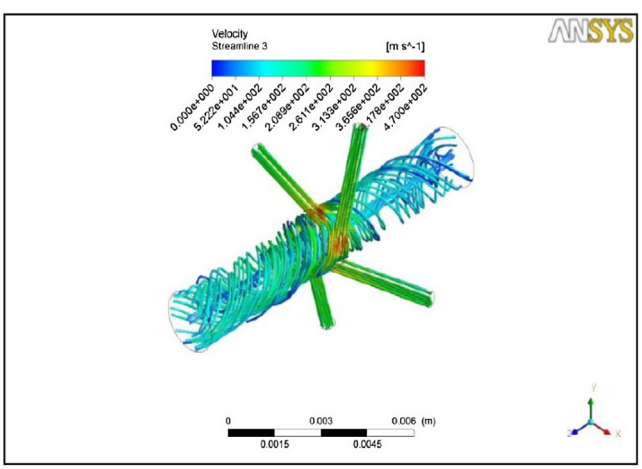

c- 3 bar

Fig. 9 Airflow behaviors inside the nozzle for different air pressure (short nozzle - injector vertical angle 15°).

the flow leaves the domain from nozzle outlet. With angle 35°, at the first part, the flow almost enters the domain from nozzle inlet except that a small IRZ appears at the peripheral and increases by increasing the pressure values. But over 2 bar it converts to a reversed flow at the peripheral. For angles 45° and 55°, the flow enters from nozzle inlet under the suction effect from injectors and leaves the domain from nozzle outlet.

Fig. 11 shows the air flow axial velocity contours for short nozzle and injector vertical angle 15° with different air pressure values from (a) 0.5 bar to (f) 3 bar. The first part is similar to long nozzle. At the second part, the flow leaves the domain from nozzle outlet. At the outlet, a sucked flow at the core is noted acting into the nozzle for a certain distance until forcing it to reverse back by the means of the main flow. It is also noted that by increasing the pressure values, the reversed mass flow sucked from the outlet decreases. The air flow axial velocity contours for short nozzle with injector vertical angle 25° with different air pressure values has a similar behavior as in short nozzle with injector vertical angle 15°.

Fig. 12 shows the air flow axial velocity contours for short nozzle with injector vertical angle 35°. The flow has a similar behavior as in long nozzle with injector vertical angle 35°, except that at the second part the IRZ converts to a reversed flow at pressure 2, 2.5 and 3 bar.

The air flow axial velocity contours for short nozzle with injector vertical angle 45° and 55°, has a similar behavior as in long nozzle with injector vertical angle 45° and 55°.

3.3. Axial velocity of air flow along nozzle length at yarn surface

Fig. 13 demonstrates the relation between the air flow axial velocity at yarn surface for long nozzle with injector vertical angle 15° and the length of the nozzle along Z axis with different air pressure values from 0.5 to 3 bar. The flow at yarn surface enters from nozzle inlet under the suction effect caused by the swirling flow from injectors. At the entrance of the nozzle approximately after z = 0.3 mm, when increasing the pressurized air value over 0.5 bar, the sucked flow at the core is subjected to a reverse flow from injectors, as explained in the axial velocity contour analysis Fig. 10.The reversed flow extension along Z axis and its axial velocity increase by increasing the air pressure values. After that the axial velocity increases towards nozzle center reaching its maximum value at injectors' zone. This maximum value increases by increasing the pressurized air value. After that the flow at yarn surface is subjected to IRZ, which previously discussed in Fig. 11. The flow's axial velocity decreases to negative values which reveal that the yarn surface is subjected to a reverse flow along this zone. After overriding the IRZ, the axial velocity increases gradually towards Z axis, and in parallel with increasing the pressure value. Until nozzle outlet, the flow diffuses very quickly to the outside causing a sudden decline in the axial velocity.

For short nozzle with injector vertical angle 15°, shown in Fig. 14, the flow at yarn surface has the same trend as previous. It enters from nozzle inlet after that the axial velocity increases towards nozzle center reaching its maximum value at injectors zone, this maximum value increases by increasing the pressurized air value, after that axial velocity decreases to negative values which reveals that the yarn surface is subjected to a reverse flow until exit from the outlet, as explained previously in Fig. 11.

For long nozzle with injector vertical angle 25°, shown in Fig. 15, the flow at yarn surface enters from nozzle inlet under the suction effect caused by the swirling flow from injectors. The axial velocity increases towards nozzle center at pressure values 0.5, 1, 1.5 and 2 bar but for 2.5 and 3 bar an IRZ

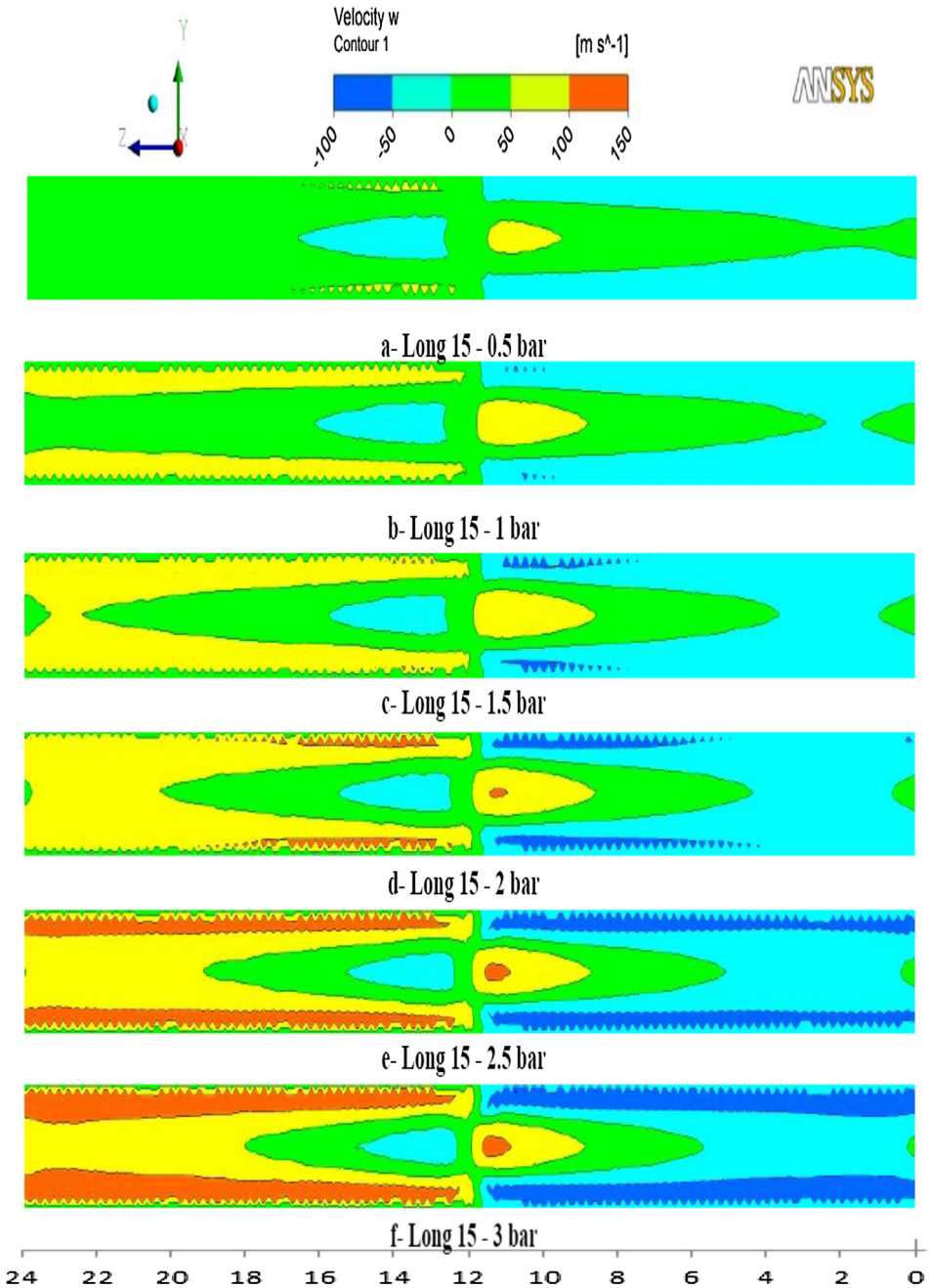

Fig. 10 Air flow axial velocity contours for long nozzle with injector vertical angle 15° with different air pressure values from (a) 0.5 bar to (f) 3 bar.

appears at 0.001 m > Z > 0.004 m. After overriding this zone, the axial velocity increases reaching its maximum value at injectors' zone. For short nozzle, the axial velocity decreases after leaving the injectors' zone to reach negative values at pressures 0.5, 1 and 1.5 bar. Then the velocity increases towards nozzle outlet until a reversed flow sucked from the outside decreases it to a negative value.

For long and short nozzles with injector vertical angles 35°, 45°, and 55°, the flow at yarn surface is almost similar to the flow with injector vertical angle 25° except a few differences. The flow at yarn surface, entered from nozzle inlet, has approximately constant axial velocity in all cases. For injector vertical angles 45°, and 55°, after pressure of 2 to 2.5 bar, axial velocity at entering starts to decline. A sudden decrease in the axial velocity is observed just before injectors zone followed by a rapid increase in the axial velocity until reaching its maximum value at injectors zone. For short nozzle with injector vertical angle 35°, at the outlet, a reversed flow sucked from the outside decreases the axial velocity to a negative value.

4. Experimental study

This paper attempts to improve yarn properties by designing various air jet nozzles and inserting them alternately to a

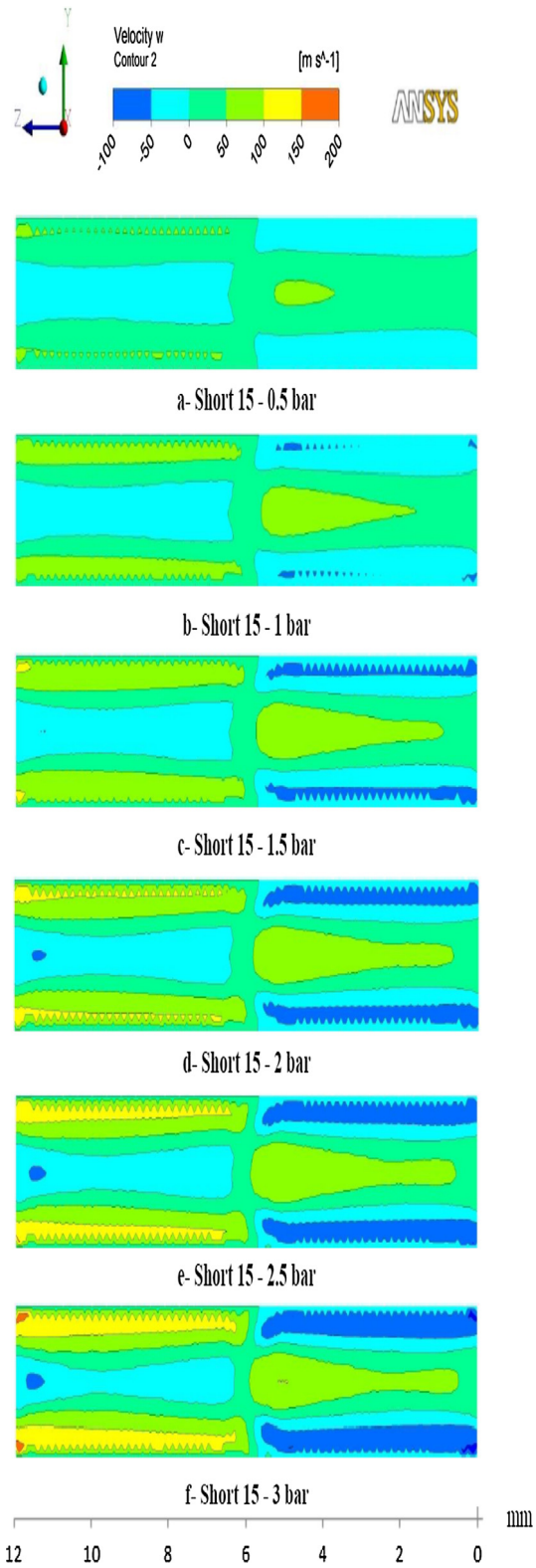

Fig. 11 Air flow axial velocity contours for short nozzle with injector vertical angle 15° with different air pressure values from (a) 0.5 bar to (f) 3 bar.

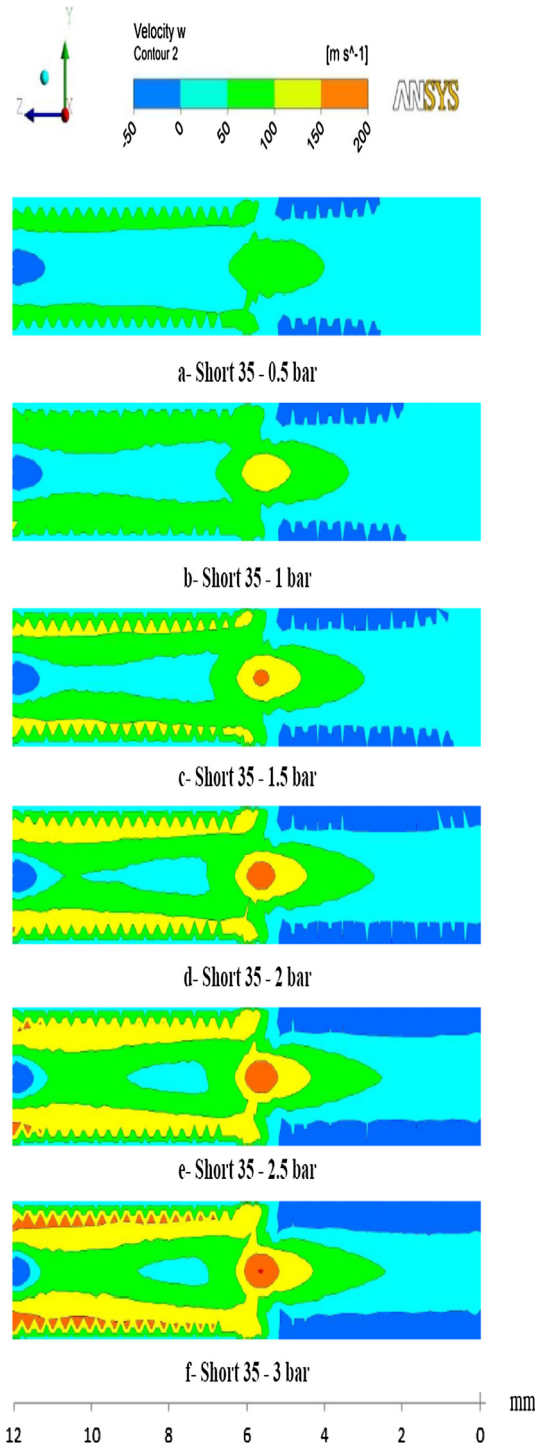

Fig. 12 Air flow axial velocity contours for short nozzle with injector vertical angle 35° with different air pressure values from (a) 0.5 bar to (f) 3 bar.

developed mechanism. This mechanism is attached to a conventional ring spinning machine to produce jet ring and modified jet ring yarns. The experiments are carried out with different processing parameters followed by an experimental study for the produced yarns characteristics.

A new set up is developed, shown in Figs. 16 and 17, representing the jet-ring and modified jet-ring spinning mechanisms respectively. The drafting system consists of a pair of delivery rollers (1-11), a double aprons area (2-21), a pair of front rollers (3-31), and a pair of extra delivery rollers (4-41). An air jet

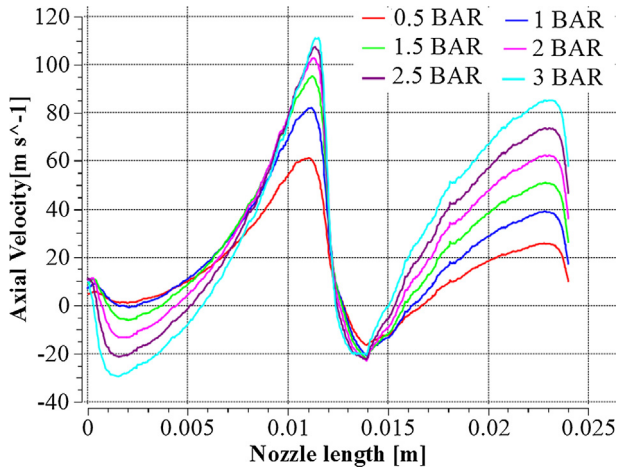

Fig. 13 Axial air velocity at yarn surface for different air pressure – Long nozzle – injector vertical angle 15°.

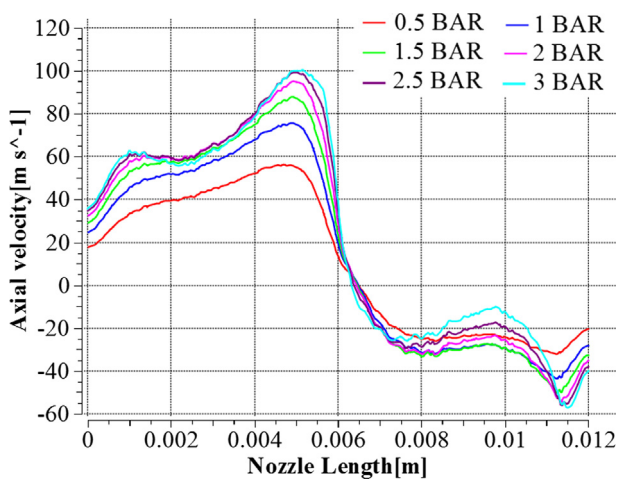

Fig. 14 Axial air velocity at yarn surface for different air pressure – Short nozzle – injector vertical angle 15°.

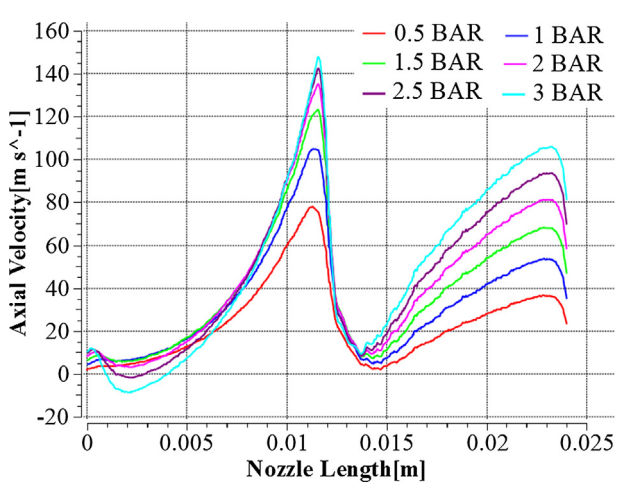

Fig. 15 Axial air velocity at yarn surface for different air pressure – Long nozzle – injector vertical angle 25°.

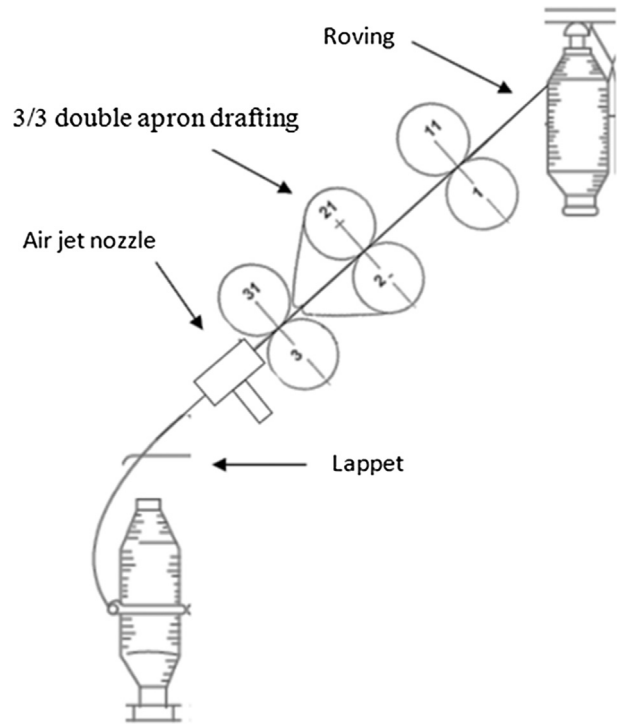

Fig. 16 Schematic of set up of the jet-ring system.

nozzle is placed in the region between the front rollers and the extra delivery rollers, such that the 3/3 draft system. Nozzle and the additional delivery rollers lay on the same axis. The roving is fed and drafted through 3/3 double apron drafting system. The drafted fibers are passed through the air jet nozzle by the means of air suction generated from the swirling air flow inside the nozzle. Fibers, coming out from the nozzle, are delivered by new additional delivery rollers, and then pass to a traveler and ring to insert, twist, and simultaneously wind the formed yarn on a bobbin.

A metal frame Fig. 18 was used to hold the nozzles, AC motor and the inverter. It controls the distance between the front rollers, nozzle and the extra delivery rollers. Also, it Controls the height of the nozzle and the extra rollers. Finally, it adjusts the balance of the mechanism.

The air-jet nozzle consists of different components. For the air suction channel, there are fibers inlet and outlet, and main and sub holes. Fig. 19 shows the structure of air jet nozzle profile. The structures of the nozzle, such as the diameters of the main and sub-holes, the number of sub-holes and angles of sub-holes (θ), have significant effects on the air-jet performance.

It's designed and manufactured, as shown in Figs. 20–22. The air nozzles are designed with the following specification: a main hole with circular cross section and constant diameter 2 mm along the main hole length, four injectors, which are tangential to circumference of the main hole. The vertical angle of the injectors with respect to the nozzle axis (θ) was 45°, Injectors have a constant diameter was 0.5 mm. They are positioned to the center of the nozzles. The air vortex directions are made in clockwise directions. The length of the nozzles (L) is 12 mm for short nozzles, and 24 mm for long nozzles.

Extra delivery rollers consist of two drafting rollers (top and bottom); the bottom roller is driven by a group of gears

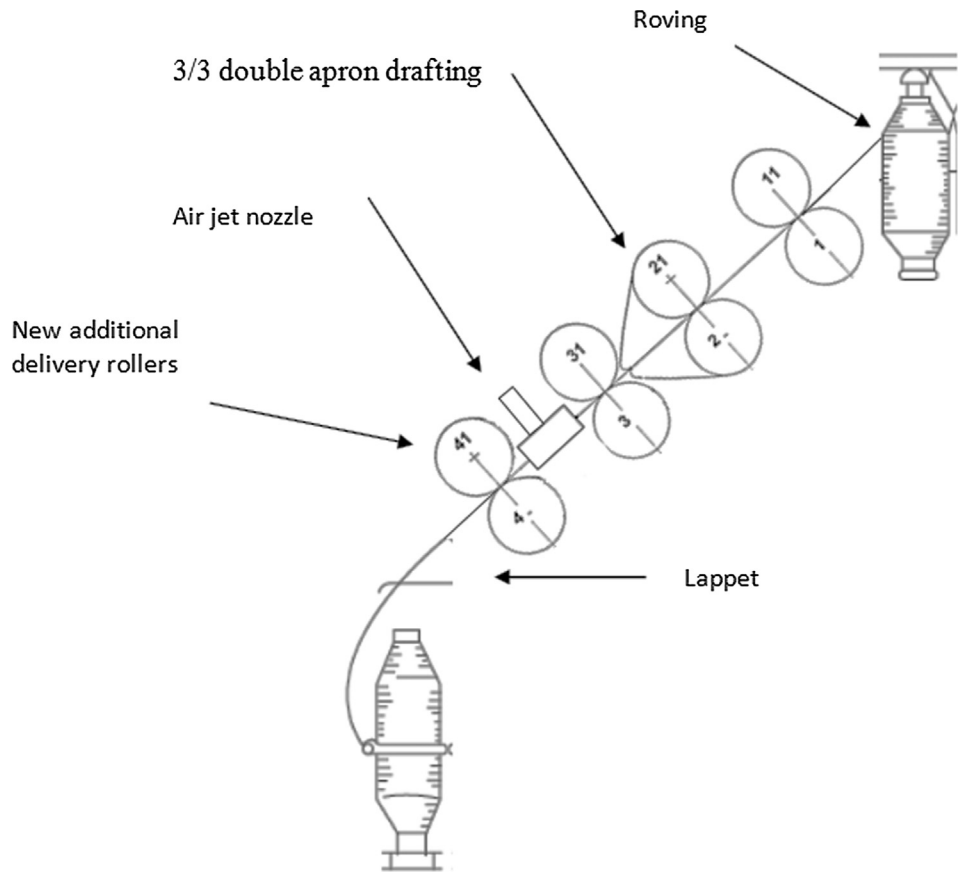

Fig. 17 Schematic of set up of the modified jet-ring system.

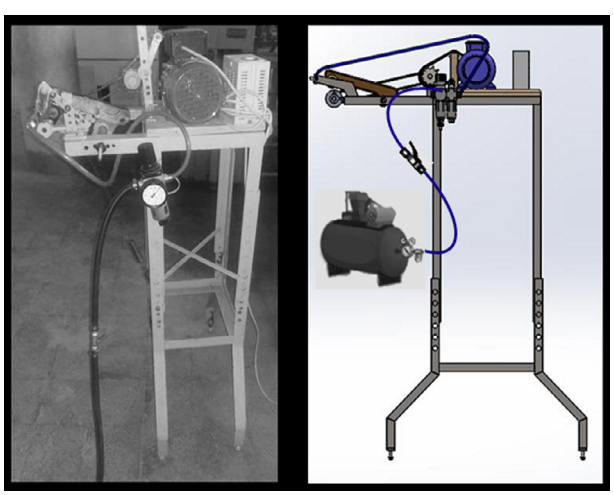

Fig. 18 Metal frame.

connected with an AC motor. The top roller is driven by the means of friction with the bottom roller. The friction between top roller and bottom roller is caused by pressure arm. The angular speed transmitted from the motor to the bottom roller is controlled by an inverter to allow changing the number of revolutions per second for the bottom roller and controlling the speed ratio between the front rollers and the extra rollers in the extra zone.

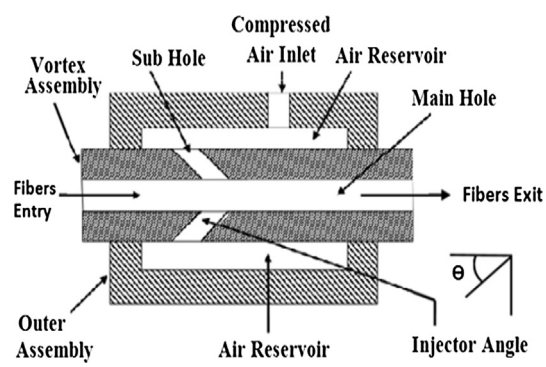

Fig. 19 General Structure of the air jet nozzle.

In compressed air systems, the electric motor operates an air compressor, which pushes more air into the system at a lower inlet pressure. Its outlet is connected to the control valve through a pipe, which controls the mass flow of air supply. Then this control valve is connected to air pressure regulator and air-filter. The air pressure regulator controls the pressure of compressed air that is supplied to the nozzle.

5. Results and discussions of the experimental study

In the present paper, Designs of Experiments of some factors (as nozzle angle **θ**, nozzle air pressure P, and nozzle length

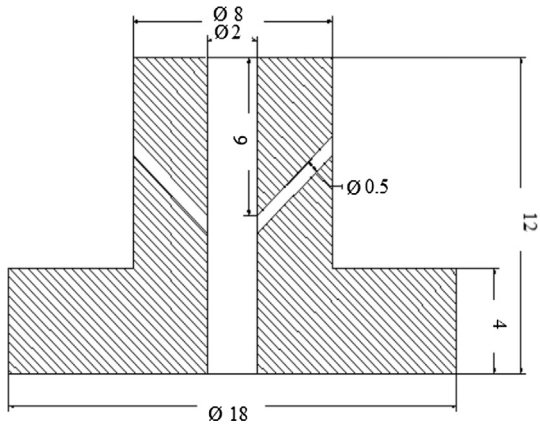

Fig. 20 Internal nozzle body (dimensions in mm).

Fig. 22 Short and long internal nozzle and external nozzle.

L) affecting the yarns properties are produced by conventional ring, jet ring and modified jet ring spinning systems are made. A combed Egyptian cotton Giza 88 is used for producing the yarns. All yarns are tested on USTER TESTER 4 and MESDANLAB Strength tester, According to Uster Standard Test Method and ASTM D2256 method.

5.1. Effect of nozzle angle (Θ) and nozzle air pressure (P) on jet ring yarn properties

Design of Experiment's details are yarn counts (Ne 20), twist factor of yarns (αe = 4.3), nozzle length (long length with 24 mm), and factors effect on yarn properties (Nozzle Angle (five values from 15° to 55°) and nozzle air pressure (six values from 0.5 to 3 bar)). Fig. 23 shows the effect of air pressure values (P) in long nozzles on the hairiness of Jet-Ring yarns for different injectors vertical angels (θ) compared with the conventional ring spun yarn. The results show that generally for all injector angles, Jet-Ring yarns have a lower hairiness values than the conventional ring spun yarn because the current swirling air inside the nozzle is capable of wrapping the protruding hairs around the yarn body. It is also observed from the results that the hairiness of Jet-Ring yarns decreases by increasing the air pressure values for all injector angles. This strong negative relation exists between the yarn hairiness and the air pressure is due to that a higher pressure values produces a higher vortex effect. So, a higher wrapping action is occurred. This supports in the CFD analysis in the previous section. From the results, it is obvious that nozzle having injectors angle of 45° produces yarn with the least hairiness, followed by 55°, 35°, 25° and the highest value is for the nozzle with angle 15°, this may be due to that injector angle of 45° has the highest axial velocity of air flow along nozzle length at yarn surface.

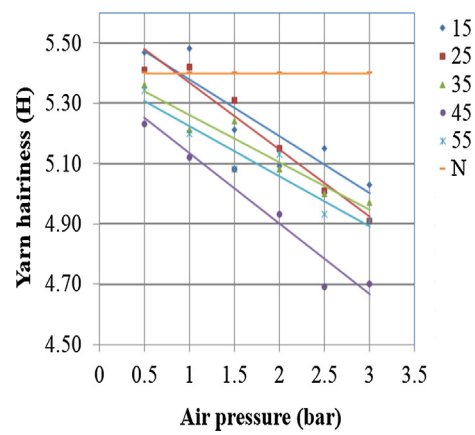

Fig. 23 Relation between air pressure of nozzle and yarn hairiness of jet ring yarn for different vertical injector angles of nozzle.

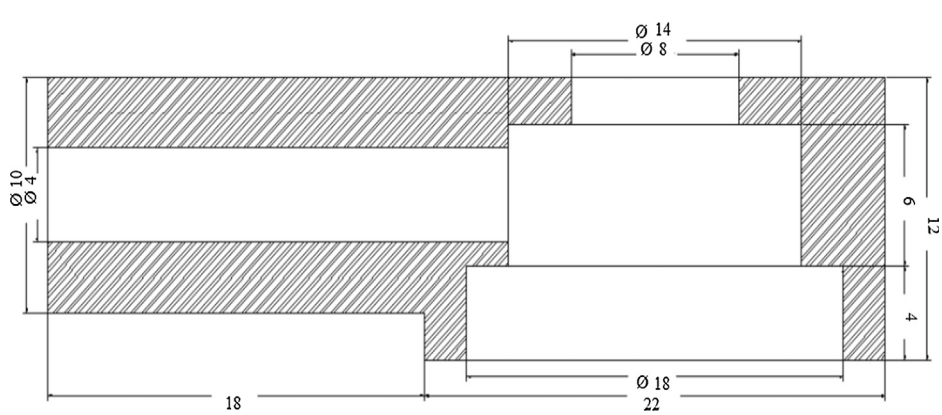

Fig. 21 External nozzle body (dimensions in mm).

Fig. 24 shows the effect of air pressure values (P) in long nozzles on the tenacity of Jet-Ring yarns for different injectors vertical angels (θ) compared with the conventional ring spun yarn. For all injector angles, the results show that the tenacity of Jet-Ring yarns increases by increasing the air pressure values until a certain pressure values after which a gradual decline is occurred. The improved tenacity is probably due to the tight wrapping of the surface fibers around the yarn body which contributes to the yarn strength, while the followed decline in strength at the high pressure values may be results from the increased tension affecting on yarn body besides the concentration of mass in a very short length brought about by the swirling action of nozzle which overall also affects the resulting yarn evenness. Jet ring yarns have a higher strength values than the normal yarns at the pressure values ranged between 1 and 2 bar for all injectors angel except for angle 15° at which probably the reversed flow, as previously explained in the CFD results, affects the fibers at the spinning triangle at the delivery zone that leads to loose fibers and subsequently decreasing yarn strength. Nozzle having injectors with vertical angle 45° produces yarn with the highest strength, followed by 55° then 35°. These results are supported by the Hairiness results which report that those angles have the most hairiness reduction values. The maximum strength value achieved is at pressure 1 bar using long nozzle with angle 45°.

5.2. Effect of nozzle length (L) and nozzle air pressure (P) on jet ring yarn properties

The effect of nozzle length (two cases short length with 12 mm, and long length with 24 mm) and nozzle air pressure (six values from 0.5 to 3 bar) on jet ring yarn properties at yarn count (Ne 20), twist factor of yarn (αe = 4.3), and nozzle Angle (θ = 45°). Fig. 25 shows the effect of air pressure values (P) in long nozzle with injector vertical angle 45° on the hairiness of Jet-Ring yarns for different nozzle lengths (L) compared with the conventional ring spun yarn. The results show that Jet-Ring yarns have a lower hairiness values than the conventional ring spun yarn. The hairiness of Jet-Ring yarns decreases by increasing the air pressure values. It is also observed from the results that in short nozzle, the hairiness value increases at pressure 3 bar which may results from great

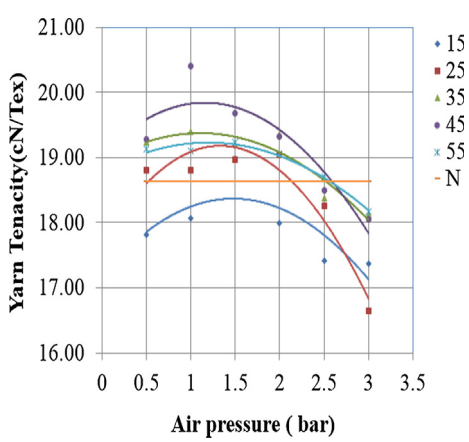

Fig. 24 Relation between air pressure of nozzle and yarn tenacity of jet ring yarn for different vertical injector angles of nozzle.

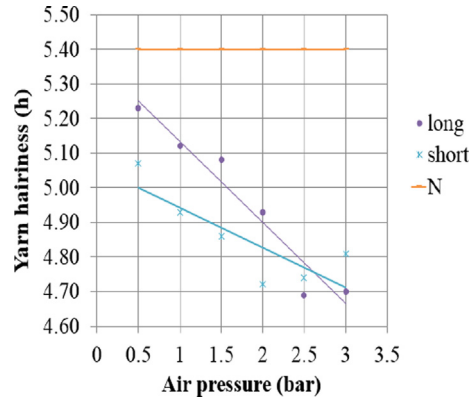

Fig. 25 Relation between air pressure of nozzle and yarn hairiness of jet ring yarn for different length of nozzle.

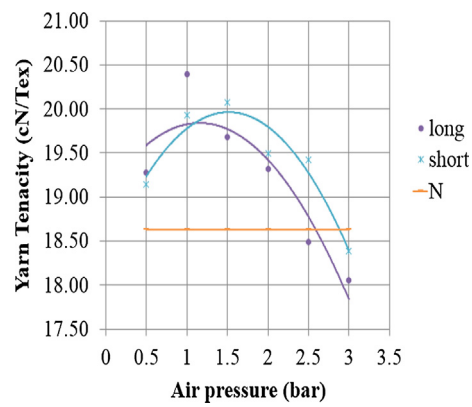

Fig. 26 Relation between air pressure of nozzle and yarn tenacity of jet ring yarn for different length of nozzle.

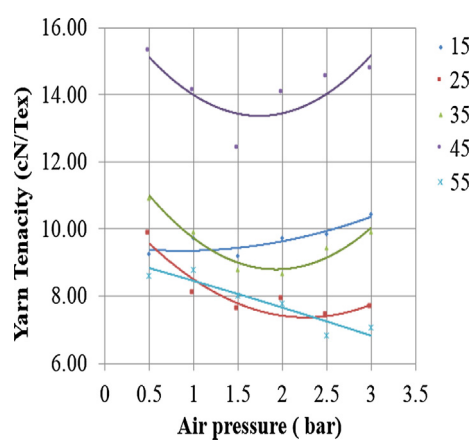

Fig. 27 Relation between air pressure of nozzle and yarn hairiness of modified ring yarn for different vertical injector angles of nozzle.

variance in the velocities at pressure 3 bar along the nozzle axis (as previously explained in the CFD analysis) which leads to decreasing the efficiency of the air vortex which overall affects the hairiness reduction. The figure also demonstrates that the hairiness of Jet-Ring yarns with short nozzle is often lower

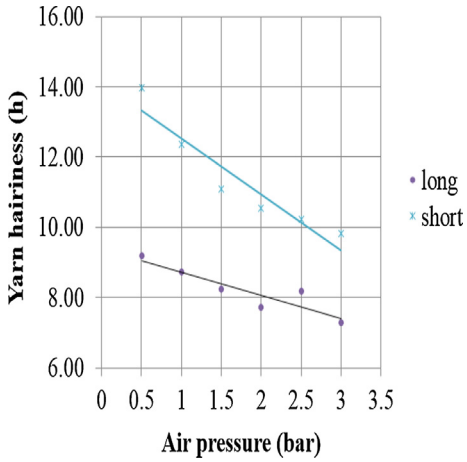

Fig. 28 Relation between air pressure of nozzle and yarn hairiness of modified ring yarn for different length of nozzle.

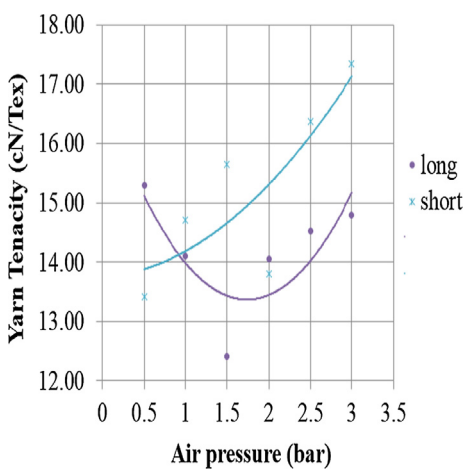

Fig. 29 Relation between air pressure of nozzle and yarn tenacity of modified jet ring yarn for different length of nozzle.

than that with long nozzle. This is may be because that the air vortex axial velocities at yarn surface with short nozzle are higher than that with long nozzle which affects the process of wrapping the fibers around yarn body and hence, controlling the hairiness reduction as stated in the CFD analysis.

Fig. 26 shows the effects of air pressure values (P) in long nozzle with injector vertical angle 45° on the tenacity of Jet-Ring yarns for different nozzle lengths (L) compared with the conventional ring spun yarn. The results show that the tenacity of Jet-Ring yarns is higher than normal yarn at pressure values ranged between 0.5 and 2.5 and lower than the normal at pressure 3 bar. The decline in strength, at the high pressure values, may be results from the increased tension affecting negatively on yarn body as discussed. In general, Jet ring yarns with short nozzle have a higher strength values than with long nozzle. These results are supported by the Hairiness results which report that short nozzle has a higher hairiness reduction values than long nozzle and subsequently higher fiber cooperation contributes to the yarn strength. For the short nozzle, the maximum tenacity value achieved is at pressure 1.5 bar.

5.3. Effect of nozzle angle (Θ) and nozzle air pressure (P) on modified jet ring yarn properties

Design of Experiment's details are yarn counts (Ne 20), twist factor of yarns and (αe = 4.3), nozzle length (long length with 24 mm), and shows the factors' effect on yarn properties (nozzle angle (five values from 15° to 55°) and nozzle air pressure (six values from 0.5 to 3 bar)). Fig. 27 shows the effect of air pressure values (P) in long nozzles on the tenacity of modified Jet-Ring yarns for different injectors vertical angels (θ). The results show that nozzle having injectors with vertical angle 45° produces yarn with the highest strength comparing with the other angles but it couldn't achieve the strength of conventional ring spun yarn. This is may be because the presence of losing control on fibers at the extra drafting zone and subsequently increasing the hairiness and C.V. mass values.

5.4. Effect of nozzle length (L) and nozzle air pressure (P) on modified jet ring yarn properties

Design of Experiment's details are yarn counts (Ne 20), twist factor of yarns and (αe = 4.3), nozzle Angle (45°), and shows the factors' effect on yarn properties (nozzle length (two cases short length with 12 mm and long length with 24 mm) and nozzle air pressure (six values from 0.5 to 3 bar)). Fig. 28 shows the effects of air pressure values (P) for nozzle with injector vertical angle 45° on the hairiness of modified Jet-Ring yarns for different nozzle lengths (L). The results show that the hairiness of modified Jet-Ring yarns decreases by increasing the air pressure values. This is may be because that by increasing the pressure values the air vortex axial velocities at yarn surface

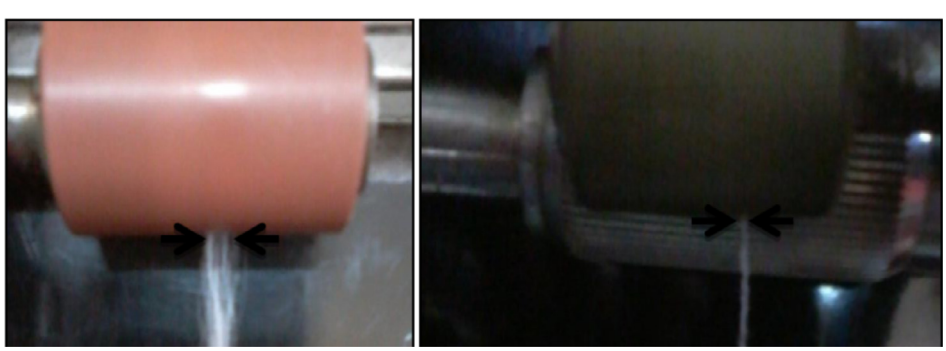

a. Ring spinning **b. Modified jet-ring**

Fig. 30 Spinning triangle size.

increase, improving the performance efficiency of the vortex as explained in the CFD analysis. The results also demonstrate that the yarn hairiness values for modified Jet-Ring yarns with long nozzle are lower than that with short nozzle. This is may be because that the air vortex axial velocities at nozzle outlet opening with short nozzle are higher than that with long nozzle, causing higher air collision with the extra drafting rollers, higher air disturbance in this zone and subsequently increasing yarn hairiness values.

Fig. 29 shows the effects of air pressure values (P) for nozzle with injector vertical angle 45° on the tenacity of New Jet-Ring yarns for different nozzle lengths (L). The results show that the tenacity of modified Jet-Ring yarns with short nozzle are higher than that with long nozzle at pressure values over 1 bar, and lower that with long nozzle at pressure values under 1 bar. Although the modified jet ring spinning succeeded clearly in reduction of spinning triangle size as shown in Fig. 30, the yarn quality of yarn produced lower than the conventional ring spinning this is may be due to some limitations in both the used ring spinning machine and mechanism. May be, some modifications in the mechanism and the machine will lead to improve the yarn properties.

6. Conclusions

- The air flow simulation using ANSYS FLUENT program plays a great role in understanding and analyzing the air flow behaviour inside the air jet Nozzles. Considering saving efforts and reducing time waste in the experimental work.
- Results show that the air flow properties inside nozzles are influenced by the injector vertical angle of air jet nozzle, nozzle length, and air pressure value.
- The recommended injector vertical angle of air jet nozzle in long nozzle is from 35° to 55°, and in short nozzle is from 45° to 55°. While, using the smaller injector vertical angles develops disturbed air flows inside their nozzles. The recommended air pressure values must not exceed 2.5 bar.
- Using the air jet nozzles in ring spinning system for producing jet ring yarns reduces yarn hairiness and improves yarn breaking force compared with ring spinning yarn. Short nozzles develop yarns with lower hairiness and higher strength than long nozzles. The injector vertical angle 45° causes the maximum reduction of hairiness, followed by angle 55° then angle 35° for Single yarn.
- In comparison with Ring spinning, the Modified jet ring spinning system succeeds in minimizing the width of the spinning triangle. But, the developed yarns have non-sufficient yarn properties. This may be due to some limitations in both the used ring spinning machine and mechanism. Some modifications in the mechanism and the machine will lead to an improvement in the yarn properties.

References

[1] S. Gordon, Y.L. Hsieh, Cotton: Science and Technology, Cambridge, Woodhead Publishing Limited, England, 2007.

[2] A.L. Carl, Fundamentals of Spun Yarn Technology, CRC Press, Boca Raton, Florida, 2003.

[3] C.A. Lawrence, Advances in Yarn Spinning Technology, Woodhead Publishing, UK, 2010.

[4] N. Haleem, X. Wang, Recent research and developments on yarn hairiness, Textile Res. J. 85 (2) (2015) 211–224.

[5] H. Stalder, A. Rusch, Successful compact spinning process, ITB Int. Text. Bull. 1 (2002) 42–43.

[6] W. Oxenham, Spinning machines at ITMA 03, JTATM 3 (2003) 1–6.

[7] K. Cheng, C. Yu, A study of compact spun yarns, Text. Res. J. 72 (4) (2003) 345–349.

[8] F. Goktepe, D. Yilmaz, O. Goktepe, A comparison of compact yarn properties produced on different systems, Text. Res. J. 76 (3) (2006) 226–234.

[9] S. Xuzhong, G. Weidong, L. Xinjin, X. Chunping, X. Bojun, Textile Numerical simulation of a three-dimensional flow field in compact spinning with a perforated drum: effect of a guiding device, Text. Res. J. 83 (19) (2013) 2093–2108.

[10] I.A. Sahito, A.A. Arbab, S.H. Jeong, Spindle speed optimization of a ring spinning machine for better surface irregularity and hairiness of yarn and fabric, Text. Sci. Eng. 52 (2015) 1–5.

[11] Z. Xia, W. Xu, A review of ring staple yarn spinning method development and its trend prediction, J. Nat. Fibers 10 (2013) 62–81.

[12] D. Yilmaz, M.R. Usal, A comparison of compact-jet, compact, and conventional ring-spun yarns, Text. Res. J. 81 (2010) 459–470.

[13] D. Yilmaz, M.R. Usal, Effect of nozzle structural parameters on hairiness of compact-jet yarns, J. Eng. Fibers Fabrics 7 (2012) 56–65.

[14] B.S. Jeon, Effect of an air-suction nozzle on yarn hairiness and quality, Text. Res. J. 70 (11) (2000) 1019–1024.

[15] D. Yilmaz, M.R. Usal, Investigation of yarn properties of modified yarn spinning systems with air nozzle attachment, Fibres Text. Eastern Eur. 21 (2) (2013) 43–50.

[16] K.P.S. Cheng, C.H.L. Li, Jet-ring spinning and its influence on yarn hairiness, Res. J. 72 (12) (2002) 1079–1087.

[17] H. Qiu, Y. Fu, Q. Luan, J. Liu, H. Jiang, Effect of airway angle of a swirl nozzle on performance of ring-spun yarn, Ind. Text. 67 (1) (2016) 10.

[18] S.N. Subramaniana, A. Venkatachalam, V. Subramaniam, Effect of some nozzle parameters on the characteristics of jet ring-spun yarns, Ind. J. Fibre Text. Res. 32 (2007) 47–52.

[19] D. Veit, Simulation in textile technology Theory and applications, Woodhead Publishing Series in Textiles: Number 136, Hardcover ISBN; 9780857090294, eBook ISBN; 9780857097088, 2012.

[20] H. Hasani, M. Hasani, Simulation approach to investigate the effect of the jet structure and air pressure on the performance of siro-jet spinning, FIBRES & TEXTILES Eastern Eur. 20 (3) (2012) 46–50.

[21] R.S. Rengasamy, A. Patanaik, R.D. Anandjiwala, Simulation of airflow in nozzle-ring spinning using computational fluid dynamics: study on reduction in yarn hairiness and the role of air drag forces and angle of impact of air current, Text. Res. J. 78 (2008) 412–420.

[22] A. Patnaik, R.S. Rengasamy, V.K. Kothari, A. Ghosh, Hairiness reduction of yarns by nozzles at ring spinning: airflow stimulation approach, J. Text. Apparel, Technol. Manage. 4 (2005) 1–11.

[23] D. Yilmaz, M.R. Usal, The effect of different nozzle configurations on airflow behaviour and yarn quality, World Acad. Sci., Eng. Technol. 6 (11) (2012) 215–219.

[24] H.F. Guo, Z.Y. Chen, C.W. Yu, Numerical study of an air-jet spinning nozzle with a slotting-tube, J. Phys.: Conf. Ser. 96 (2008) 1–5.

[25] "Chapter10 Modeling Turbulence", Fluent Inc., 2001. Accessed (1/10/2014) http://www.afs.enea.it/fluent/Public/Fluent-Doc/PDF/chp10.pdf.